Numerical Method for 2D and 3D Viscous Flows

P. R. Dodge*
AiResearch Manufacturing Company of Arizona, Phoenix, Ariz.

A numerical method is presented that offers rapid solutions to the Navier-Stokes equations for even the most complicated geometries. It is based on separating the momentum and continuity equations into coupled elliptic and parabolic groups. A rapid iteration occurs between equations. Examples are presented for 3D flow in turbine stators. Good agreement is obtained for experimental loss and heat-transfer coefficients.

I. Introduction

INTERNAL flow devices currently in use in turbomachinery are among the most complicated fluid dynamic devices to analyze. In the past, the lack of fundamental predictive methods has led to reliance on experiments. However, recent progress in numerical methods is now leading towards the substitution of analysis for experimentation. Nevertheless, methods for solutions to equations, complete enough to include the significant viscous and pressure force effects have been too time-consuming to prove practical. Until recently, effort has been concentrated on the use of simplified forms of the Navier-Stokes equations.

One of the early significant efforts in this light was that of Wu,[1] where inviscid equations in three dimensions are reduced to coupled sets of two-dimensional solutions. The radial equilibrium portion of this solution can be cast essentially as subsonic by specifying the swirl as one coupling term. A numerical method for this particular equation, utilizing curvature of streamline methods, was developed by Smith.[2] Subsonic blade-to-blade solutions were developed by Katsanis and McNally.[3] Transonic solutions utilizing time-dependent methods were developed by Gopalakrishnan and Bozzola,[4] and McDonald.[5] Transonic relaxation solutions have been developed by Dodge.[6] Inviscid solutions to fully three-dimensional flow in turbomachine components have been developed by Denton,[7] utilizing time-dependent methods.

Viscous solutions have taken one of three directions. The first is that of boundary-layer techniques such as those of Hirsch.[8] The second is that of following the kinematic transport of vorticity, such as applied by Lakshminarayana.[9] The third is to parabolize the Navier-Stokes equations by restricting or eliminating upstream influence. A most recent example of this is the work of Pratap, Majumdar, and Spalding.[10]

All of these methods suffer from inadequacy in describing the flow processes in turbomachinery. The inviscid methods, although useful, do not begin to provide predictions of loss and heat transfer and the effects of these on the mainstream flow. The parabolic methods allow no recognition of upstream influence. Serious and substantial effects of surface curvatures and downstream blockages are ignored. Time-dependent solutions to the Navier-Stokes equations, although theoretically possible, are beyond current computer hardware capabilities. The following discussion describes the development of a method that overcomes many of the objections to past techniques. This method will allow efficient solution of the Navier-Stokes equations in complete enough form to accurately predict significant viscous-flow interactions over a wide variety of practical situations.

Presented as Paper 76-425 at the AIAA 9th Fluid and Plasma Dynamics Conference, San Diego, Calif., July 14-16, 1976; submitted July 22, 1976; revision received March 10, 1977.
Index category: Computational Methods.
*Senior Engineering Specialist.

II. Basic Equations

The Navier-Stokes equations for turbulent flow are often closed by assuming that an effective viscosity can be used to describe the effects of Reynolds stresses. If this is true, then the incompressible form can be written as in Eq. (1).

$$\frac{DW}{Dt} = -\frac{\nabla p}{\rho} + \nabla \cdot [\nu_e(\text{def } W)] \tag{1}$$

where def $W = \nabla W + (\nabla W)^*$
W = the velocity vector
p = the static pressure
ρ = the density
ν_e = the effective kinematic viscosity

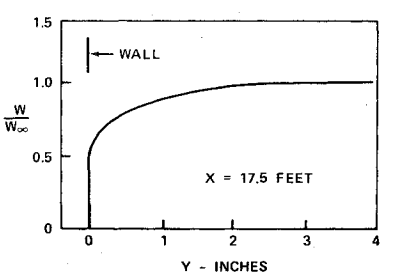

Fig. 1 Velocity profile NACA shaped test body.

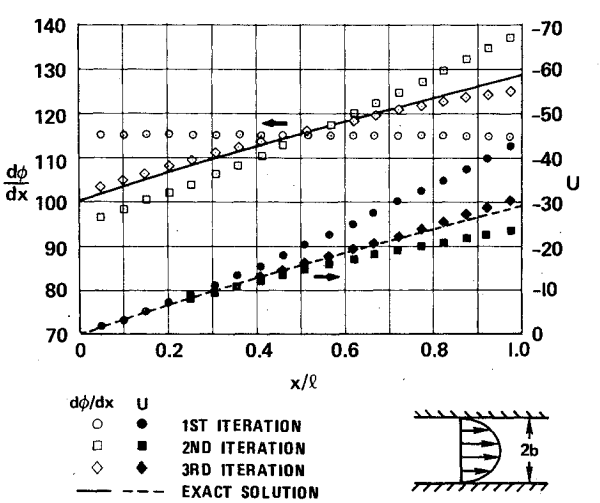

Fig. 2 Velocity components on centerline versus x/ℓ, $8\nu^2\ell/Ab^4 = 0.66668$.

This equation becomes difficult to solve because of its extreme nonlinear nature.

At high Reynolds number, the velocity distribution near the wall appears to the casual observer as nearly discontinuous. As an example, consider Fig. 1 for the boundary layer 17.5 feet down a shaped body (from Schubauer and Klebanoff).[11] The presence of extreme rates of change near the walls requires either extremely closely spaced nodes or wall functions such as those used by Pratap et al.[10] Nevertheless, the details of the flowfield in the near-wall region can have substantial effects on the outer region of the boundary layer and even the freestream. An attempt to solve Eq. (1) directly by relaxation techniques requires many nodes with several dependent variables. Besides the obvious impact on required computer capacity, the convergence characteristics of such a process become progressively poorer as the problem size increases (Dodge[12]). Nevertheless, the pressure field plays a great role in the transport of vorticity in the regions adjacent to the wall and must be considered.

To permit an optimization of numerical methods, the velocity can be separated into its viscous and potential components.

$$W=\nabla\phi+U \tag{2}$$

An additional dependent variable is introduced in so doing. Substitution of Eq. (2) into Eq. (1) (for steady flow) will result in Eq. (3).

$$(U\cdot\nabla)U+(\nabla\phi\cdot\nabla)U+(U\cdot\nabla)\nabla\phi+(\nabla\phi\cdot\nabla)\nabla\phi$$
$$=-\frac{\nabla p}{\rho}+\nu_e\nabla^2U+\nu_e\nabla(\nabla^2\phi)+(\text{def } U)\nabla\nu_e$$
$$+[\text{def}(\nabla\phi)]\nabla\nu_e \tag{3}$$

Since a somewhat arbitrary dependent variable has been introduced, assumptions consistent with the irrotationality of the potential function can be introduced. For Eq. (3), a suitable assumption is to equate purely potential terms to the pressure gradient.

$$(\nabla\phi\cdot\nabla)\nabla\phi=-\nabla p/\rho \tag{4}$$

It can be shown that for any positive pressure field, p, a potential must exist that satisfies Eq. (4). Thus, Eq. (3) can be reduced to Eq. (5).

$$(W\cdot\nabla)U+(U\cdot\nabla)\nabla\phi=\nu_e\nabla^2U+\nu_e\nabla(\nabla^2\phi)$$
$$+(\text{def } U)\nabla\nu_e+2[\nabla(\nabla\phi)]^*\nabla\nu_e \tag{5}$$

Since this equation alone is not sufficient, a second equation for potential is obtained from continuity.

$$\nabla^2\phi=-\nabla\cdot U \tag{6}$$

Equation (6) is an obvious candidate for solution by relaxation. Since the result is a potential gradient, relatable to a pressure gradient through Eq. (4), the grid can be relatively sparse near the wall, yielding a practically sized relaxation problem.

Equation (5) would be parabolic, with a dominant direction in the flow direction, except for streamwise diffusion. For anything but the lowest Reynolds numbers, it is a reasonable assumption to ignore streamwise diffusion of momentum. Although there are viable alternatives to doing this, all numerical calculations reported herein include this assumption. As a consequence of the parabolic nature, Eq. (5) is a candidate for a form of marching solution similar to those used for boundary-layer analyses. Since both equations contain coupling terms, iteration must be carried out between Eqs. (5) and (6).

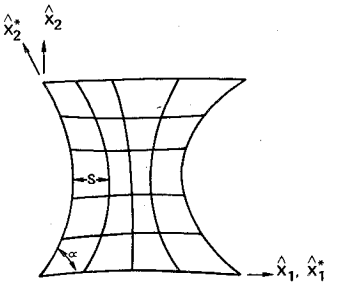

Fig. 3 Nonorthogonal grid systems, x_1-x_2 plane.

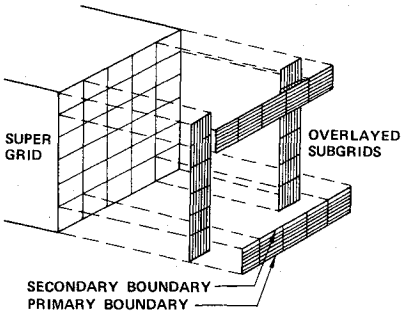

Fig. 4 Grid system structure.

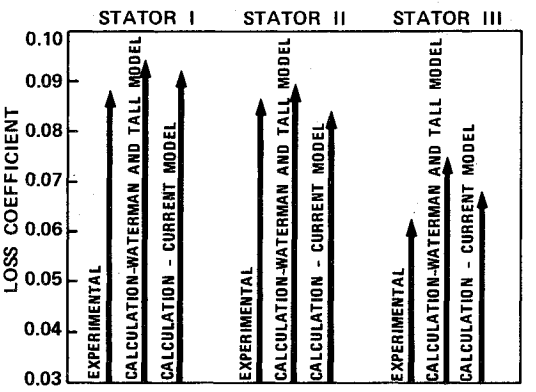

Fig. 5 Overall energy loss coefficient for three stators of Waterman and Tall.

Boundary conditions for Eq. (5) consist of an inlet profile and the no slip condition at the walls. Thus at the wall U is equated to the negative of the potential gradient. The potential boundary conditions (Eq. 6) can be somewhat more complicated. However, for all cases described herein, a condition that the gradient of potential normal to the wall is zero suffices. It should be noted that this does not imply that the pressure gradient normal to the wall is zero, since pressure is related to the magnitude of the potential gradient.

Upstream and downstream boundary conditions use a specified constant potential, zero at the inlet and an input value at the exit.

Simple Example

To study the form this iteration takes, it is useful to examine a simple case. Consider the flow of a laminar fluid between two parallel plates. The Navier-Stokes equations reduce to a linear equation given by Eq. (7).

$$dp/dx=\mu(\partial^2W/\partial y^2) \tag{7}$$

$$W=0; \qquad y=\pm b \tag{8}$$

where μ is the viscosity, x is the position in the streamwise direction, and y is the cross-channel dimension. Equations (4) and (5) reduce to Eq. (9) and (10), respectively.

$$\frac{d\phi}{dx}\frac{d^2\phi}{dx^2} = -\frac{1}{\rho}\frac{dp}{dx} \tag{9}$$

$$U\frac{d^2\phi}{dx^2} + W\frac{\partial U}{\partial x} = \frac{\mu}{\rho}\frac{\partial^2 U}{\partial y^2} \tag{10}$$

Even though the Navier-Stokes equations result in a linear solution, the split equations do not. Nevertheless, Eqs. (9) and (10) have an analytical solution given by Eqs. (11) and (12).

$$\phi(x) = \frac{b^6A^2}{24\nu^3}\left\{\left[\frac{8\nu^2x}{Ab^4}+1\right]^{3/2}-1\right\} \tag{11}$$

$$U(x,y) = \frac{b^2A}{2\nu}\left[\left[1-\left(\frac{y}{b}\right)^2\right]-\left[\frac{8\nu^2x}{Ab^4}+1\right]^{1/2}\right] \tag{12}$$

$$A = -\frac{1}{\rho}\frac{dp}{dx} = \frac{d\phi}{dx}\frac{d^2\phi}{dx^2} \tag{13}$$

A numerical solution would, however, proceed from a relaxation solution of Eq. (14) followed by a marching solution of Eq. (10).

$$\frac{d^2\phi}{dx^2} = -\frac{\partial U}{\partial x}\Big)_{y=0} \tag{14}$$

Successive over-relaxation was used for Eq. (14) with a second-order implicit solution to Eq. (10). Results for the variation of centerline velocity are shown in Fig. 2. Since the total velocity must be constant, ultimately the sum of potential and viscous components must be constant. An increase of the potential derivative results in the static pressure drop required to actually drive the flow. The initial assumption was a constant potential velocity. Three iterations between marching and relaxation equations were required to effect convergence to a reasonable agreement with the analytical solutions. This suggests that in practice the coupled iteration should be expected to proceed rapidly.

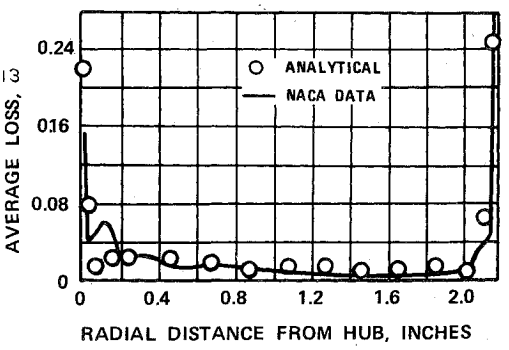

Fig. 6 Radial distribution of loss for NACA TN 2871 turbine stator.

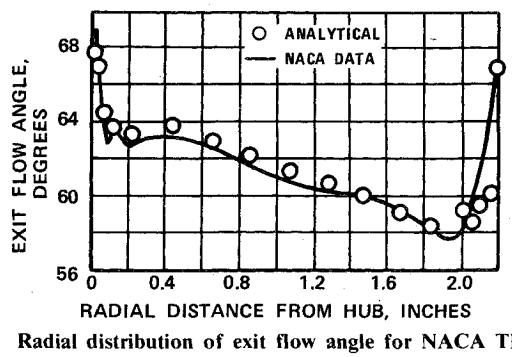

Fig. 7 Radial distribution of exit flow angle for NACA TN 2871 turbine stator.

3D Numerical Methods

The method discussed above has been implemented in a three-dimensional program capable of handling blade rows of arbitrary 3-D shapes. It is not possible, herein, to describe this program and its detailed methods. However, a few features are worth mentioning. A basic relaxation grid is established that has boundaries coincident with the geometric boundaries of the blade row. Equations (5) and (6) are expanded in a full curvilinear set. Since, in general, turbomachinery blades do not intersect hubs and shrouds at right angles, a further transformation into a nonorthogonal grid system is required (see Fig. 3). The solution grid system is X_1^*, X_2^*, X_3. Successive X_3 planes are orthogonal as indicated by Eq. (15),

$$K(\hat{X}_1^* \times \hat{X}_2^*) = (\hat{X}_1 \times \hat{X}_2) = \hat{X}_3 \tag{15}$$

where $\hat{X}_i$ is a unit vector in the ith direction, and $\hat{X}_1^*$ is in the direction of $\hat{X}_1$. The result is that derivatives with respect to $\hat{X}_1$ or $\hat{X}_2$ can be expressed as functions of $\hat{X}_1^*$ and $\hat{X}_2^*$; the normal transformation coefficients, h_1, h_2, and h_3; along with two parameters describing the nonorthogonality.

Actual solution is, however, for velocity components in the orthogonal directions, not in the grid system direction. Near the boundaries, additional coupled subgrids are introduced. These grids are spaced nonlinearly near the wall. Spacings as much as three orders of magnitude smaller near the wall, than that nearest the center of the passage, are utilized. These grid systems are shown schematically in Fig. 4. The solutions for each subgrid are carried out independently and coupled at their boundaries by a process similar to that reported by Steger and Lomax.[13] The turbulence model utilized to date is algebraic. It contains the following elements: mixing length near the wall with van Driest's wall shear correction, and the Cebeci-Smith pressure corrections; transition to a constant freestream turbulent kinematic viscosity away from the wall; and transition to nearly constant viscosity in the wake. The code itself is primarily Fortran, approximately 16,000 card images long, requiring 50,000 octal words of core memory, and 1 to 2 million words of disk storage. Run time on a CDC 6400 is approximately one hour per case. A typical grid system results in 2 to 6 thousand relaxation nodes, and 20 to 30 thousand marching nodes.

Separation

When a flow reversal occurs, Eq. (5), although still parabolic, becomes a non-well-posed initial value problem. All forward marching differences then become unstable. When this occurs, there are at least three ways to preserve the structure and advantage of this numerical method: 1) Assume that no significant convection in the main flow direction occurs in a reverse-flow region; 2) Switch the difference star to one extended in the forward direction. This requires the use of previously calculated values of dependent variables; 3) Transform the equations into a function space using spectral methods and proceed to solve the set as a non-well-posed problem.

Methods (1) and (2) have been used by Carter and Wornom[14] for the boundary-layer equations. Method (1) is utilized for the three-dimensional calculations displayed subsequently. It is a reasonable physical assumption as long as the separation bubble is modest in extent. This is the norm for efficient turbomachinery devices. Method (3) has been used by Dodge and Lieber[15] for two-dimensional calculations. It has, as well, the dubious advantage of treating streamwise diffusion of momentum.

III. Typical Results

Results for three turbine cascades using an earlier turbulence model (without Cebeci-Smith correction and freestream turbulence model) were reported by Waterman and Tall.[16] Figure 5 shows a comparison of overall loss

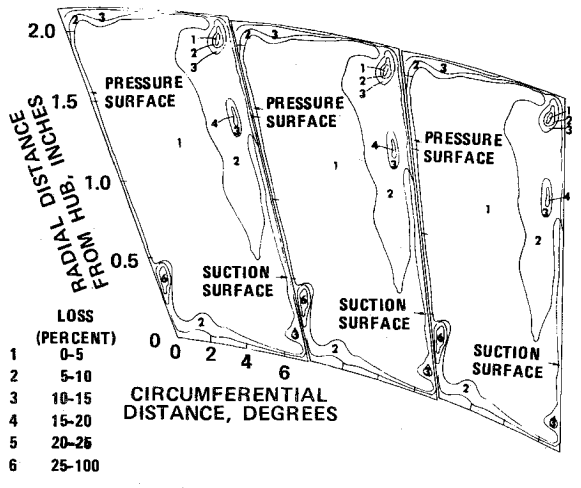

Fig. 8 First iteration (parabolized solution) contours of constant loss of NACA TN 2871 turbine stator.

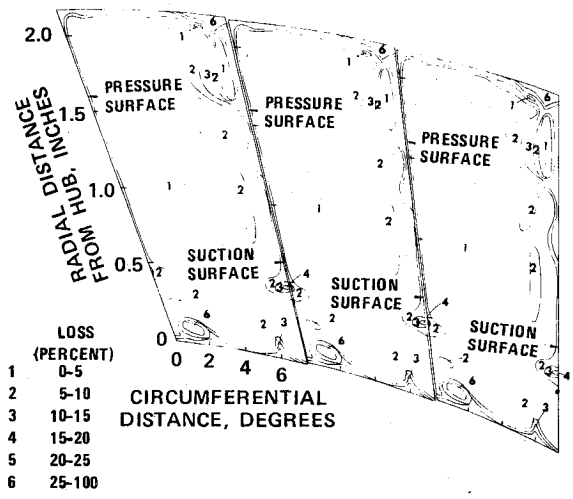

Fig. 9 Third iteration contours of constant loss for NACA TN 2871 turbine stator.

coefficients. The inclusion of pressure and freestream turbulence effects results in improved universality. Figures 6 and 7 show a comparison of loss distribution and exit flow angle for a high-aspect-turbine stator reported by Allen et. al.[17] Excellent agreement between calculation and experiment is obtained.

Figures 8 and 9 show, for this case, the result of the iteration on coupling terms. These calculations can be compared to the measured values shown in Fig. 10. First-pass results are essentially that of a parabolic solution. Subsequent passes result in what appears to be only minor modifications of pressure distributions. However, these readjustments of pressure distributions have a substantial effect, as can be seen, on the viscous solutions. As iteration continues, unrealistically high losses near the tip converge to a distribution more closely approximating the data.

Heat Transfer

The inclusion of an energy equation into the parabolic set, represented by Eq. (5), allows for the examination of heat-transfer coefficients. A simple energy equation is used, neglecting viscous dissipation. Heat flux is related to the effective turbulent kinematic viscosity through a turbulent Prandtl number set at 0.8. The turbine stator investigated by Blair[18] was analyzed using this method. The computed distribution of endwall heat-transfer coefficients is shown in Fig. 11a as lines of constant Stanton number. The

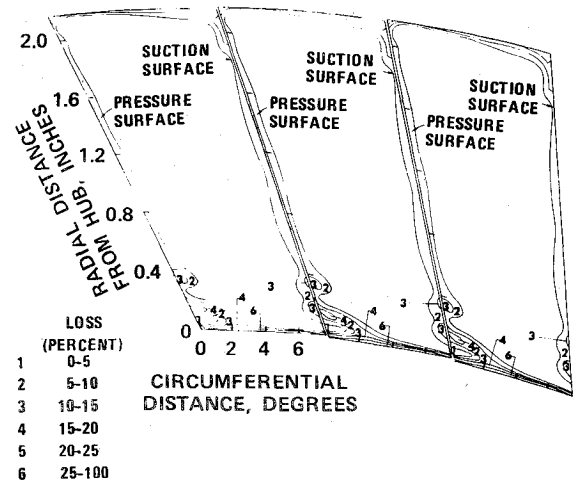

Fig. 10 Measured contours of constant loss for NACA TN 2871 turbine stator.

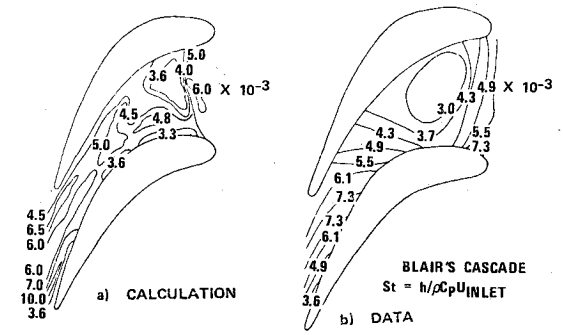

Fig. 11 Endwall heat-transfer coefficients.

measurements reported by Blair are shown in Fig. 11b. Agreement is quite good, both quantitatively and qualitatively.

Note the following comments. Low heat-transfer coefficients near the suction surface trailing edge are clearly shown. Low coefficients near the entrance of the cascade toward the pressure surface are predicted, although the experimental region is somewhat lower in level and larger in extent. A region of low heat transfer was predicted near the suction surface at approximately one-third chord. Calculation indicates a slightly lower value than the data. High coefficients are evident at the cascade exit in midchannel. Calculated peaks are higher, but the rates of change are such as to make experimental resolution difficult.

IV. Conclusion

A numerical method has been presented that results in rapid solutions to the Navier-Stokes equations. Run times, even for very complex geometries, are sufficiently rapid to make the resulting solutions practical for design as well as research tasks. Extensions to compressible flow, through not treated herein, follow with only minor modifications to the basic method.

V. Acknowledgments

The author is grateful to R.B. Pope who assisted in the debugging and development of the turbulence model of the 3D Program, and S.L. Slemmons who contributed to the coding of the 3D Program.

References

[1]Wu, C.H., "A General Theory of Three-Dimensional Flow with Subsonic and Supersonic Velocity in Turbomachines Having Ar-

bitrary Hub and Casing Shapes – Parts I and II," ASME Paper 50-A-79.

[2]Smith, L.H. Jr., "Radial-Equilibrium Equations of Turbomachinery," ASME 65-WA/GTP-1.

[3]Katsanis, T. and McNally, W.D., "Fortran Program for Calculating Velocities in a Magnified Region on a Blade-to-Blade Stream Surface of a Turbomachine," NASA TN D-5091.

[4]Gopalakrishnan, S. and Bozzola, R., "A Numerical Technique for The Calculation of Transonic Flows in Turbomachinery," ASME Paper 71-GT-42, Houston, Texas, 1971.

[5]McDonald, P.W., "The Computation of Transonic Flow Through Two-Dimensional Gas Turbine Cascades," ASME Paper 71-GT-89, Houston, Texas, 1971.

[6]Dodge, P.R., "A Non-Orthogonal Method for Solving Transonic Cascade Flows," ASME Paper 76-GT-63, New Orleans, La., 1971.

[7]Denton, J.D., "A Time Maching Method for Two- and Three-Dimensional Blade-to-Blade Flows," Marchmood Engineering Laboratories Report R/M/R215.

[8]Hirsch, C., "Flow and Performance Prediction in Axial Flow Compressors Including Endwall Boundary Layers," ASME Paper 76-GT-72, New Orleans, La., 1976.

[9]Lakshminarayana, B., "Methods of Predicting the Tip Clearance Effects in Axial Flow Turbomachining," ASME Paper 69-WA/FE-26, Los Angeles, Calif., 1969.

[10]Pratap, V.S., Majumdar, A.K., and Spalding, D.B., "Numerical Computation of Flow in Rotating Ducts," ASME Paper 76-FE-25.

[11]Schubauer, G.B. and Klebanoff, P.S., "Investigation of Separation of The Turbulent Boundary Layer," NACA TN 1030.

[12]Dodge, P.R., "Transonic Relaxation Methods," Notes from von Karman Institute Lecture Series 84, Feb. 1976.

[13]Steger, J.L. and Lomax, H., "Calculation of Inviscid Shear Flow Using a Relaxation Method for the Euler Equations," NASA SP-347.

[14]Carter, J.E. and Wornom, S.F., "Solutions for Incompressible Separated Boundary Layers Including Viscous-Inviscid Interactions," NASA SP-347, March 1975.

[15]Dodge, P.R. and Lieber, L.S., "Separated Flow Program for Office of Naval Research," AiResearch Report 74-211196(5), Feb. 1976.

[16]Waterman, W.F. and Tall, W.A., "Measurement and Prediction of 3D Viscous Flows in Low-Aspect-Ratio Turbine Nozzles," ASME Paper 76-GT-73, New Orleans, La., 1976.

[17]Allen, H.W., Kofskey, M.G., and Chomnes, R.E., "Experimental Investigation of Loss in Annular Cascade of Turbine-Nozzle Blades of Free Vortex Design," NACA TN 2871, 1952.

[18]Blair, M.F., "An Experimental Study of Heat Transfer and Film Cooling on Large-Scale Turbine Endwalls," *Transactions of The ASME, Journal of Heat Transfer*, Series C, Vol. 96, Nov. 1974, pp. 524-529.